Automatic Lens Identification for Thermographic Cameras

Robin Paul Swoboda*, Robert Bergmann†, Frank Reifegerste* and Jens Lienig*
*Institute of Electromechanical and Electronic Design, Dresden University of Technology, Germany
†Infrared Sensor Technology and Measurement Division, InfraTec GmbH [1], Germany
https://orcid.org/0009-0006-4713-1544, r.bergmann@infratec.de, frank.reifegerste@tu-dresden.de, jens@ieee.org

***Abstract*—Measuring high-resolution thermographic images requires accurate radiometric calibration (assignment of temperature to measured value) of the camera to the optics used. The lenses in particular have a significant influence on this calibration. Infrared (IR) cameras without automatic detection of the attached lens are prone to errors when selecting the correct calibration range after a manual lens change. In order to address this problem, a reliable and user-friendly approach is introduced to minimize errors due to lens mix-ups or incorrect operation by the customer and during in-house calibration. This is achieved by developing a system for automatic lens identification on thermographic cameras. To this end, contactless and contact-based variants of lens-body data transmission are researched and evaluated to application-specific criteria. Functional tests of a contactless radio-frequency identification (RFID) solution delivered very reliable data transmission results and demonstrated the possibility to incorporate the method in a prototype.**

***Index Terms*—Thermography, Infrared, Automatic lens identification, Lens-body-interface, Camera-lens-communication.**

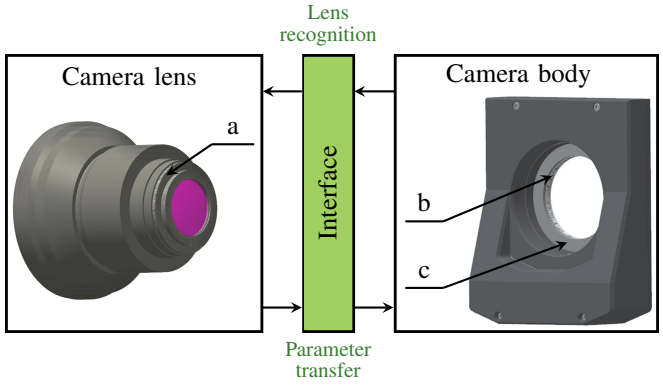

Fig. 1. Overview of the lens–body camera system. Elements in green mark the contributions of this paper. Subfigures (a)–(c), which are referenced in chapter IV, show the lens contact surface, the M60 lens mount, and the corresponding contact ring/surface of module 0, respectively.

I. Introduction

IR radiation, emitted by all objects above absolute zero kelvin (-273.15 °C), forms the basis of temperature detection in infrared camera systems. These systems enable precise surface temperature measurements with low uncertainty and are indispensable in modern thermal analysis. However, to achieve accurate results, radiometric calibration of the camera-lens system is usually conducted for all parameter settings/optics. This process, typically conducted by the manufacturer, involves selecting numerous calibration parameters, such as calibration factors, and is prone to human errors when performed manually [2]. To address this issue, the work focuses on the development of an automated lens identification system offering compatibility with thread mount interfaces. Thermography cameras often implement lenses from different manufacturers. Therefore, the identification mechanism of lenses should be easily adaptable to a broad range of lens designs, focusing on the M60 lens mount in this particular case. Although the thread mount lenses are usually not mechanically adaptable, they can be extended using technological enhancements.

The contributions of this paper (Fig. 1) include: (a) the development of an automatic lens-body interface, (b) reliable lens detection, (c) streamlined parameter transfer to enhance operational efficiency for end users, and (d) reduced calibration errors in professional infrared measurement applications. This is achieved by investigating existing mechanical and electrical lens-connection methods (Section II) as well as suggesting and evaluating potential approaches (Section IV, V) to be compatible with the camera system. As a result, the most reliable method is implemented as a functional demonstrator, providing practical validation of the concept (Section VI).

II. State of the Art

Radiometric calibration ensures accurate temperature measurement for IR cameras by converting a sensor signal into radiation intensity or temperature. Calibration is performed by comparing imaging blackbody calibration sources with known temperature and emissivity. Thus, one can derive lens-specific calibration tables that account for transmission losses and temperature drift. Without such calibration, only non-radiometric imaging is possible, making precise temperature readings impossible [2]. Current IR cameras with screw-mounted lenses require manual entry of lens data such as type or serial number. This limitation also extends to users, as the system cannot automatically identify incompatible lenses or warn about measurement errors following lens changes.

A. Lens identification approaches for VIS

From the previous paragraph, the need for an automatic lens identification method is evident. In the past, multiple approaches for lens connection and automatic lens detection during connection have been developed. For visible imaging system (VIS) cameras there exist four approaches (Fig. 2) [3].

This is the personal version of the paper created by the authors. Please cite as:
R. P. Swoboda, R. Bergmann, F. Reifegerste, J. Lienig "Automatic Lens Identification for Thermographic Cameras," 13th Int. Conf. on Control, Mechatronics and Automation (ICCMA 2025), Paris, France, Nov. 2025.

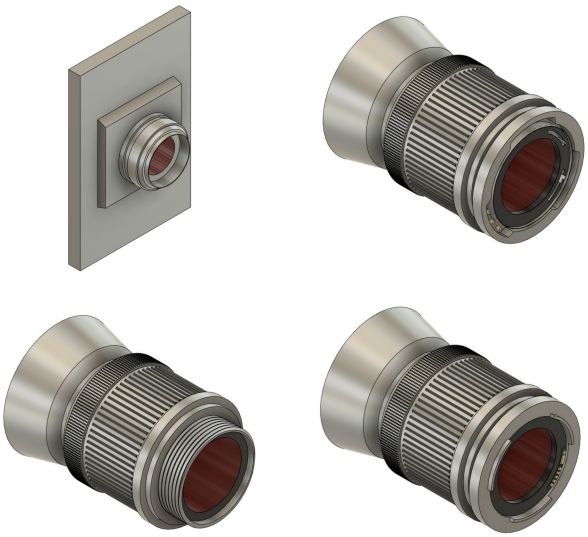

Fig. 2. Abstracted illustration for generic lens connection variants of VIS cameras designed by the author. From upper left-hand corner to lower right-hand corner: whole-plate interface, bracket mount interface, thread mount interface and bayonet interface.

The rectangular plate mount used from the 19th century to the 1920s, fixed the lens onto a plate that was inserted into the camera body [4]. This was succeeded by the clamp ring mount embodied by early Canon FD lenses, where a ring was tightened around the lens to secure it. Later, the thread mount allowed lenses to be directly screwed into the camera body; although still used in static configurations, this system is prone to loosening under movement. Currently, the bayonet mount is the widely used solution due to its secure, wear-resistant, and user-friendly interface that supports both mechanical and electrical contacts [3].

The origins of automatic lens identification lie in mechanical systems designed to transmit data between lens and camera. Early examples include Nikon's F-mount and Canon's FL/FD mounts, which provided parameters, like aperture settings, mechanically for optimized exposure [5], [6]. The M42 thread also supported features such as open-aperture measuring using a cam mechanism [7], [8]. The 1980s marked a major shift towards electronic data transmission. Canon's T80/T90 series introduced the EF mount, and Minolta's 7000 model featured the A-mount, the first single-lens reflex (SLR) camera with fully automatic auto-focus (AF). These systems enabled bidirectional communication for transmitting lens data such as AF, exposure, and aperture, thereby eliminating the need for mechanical coupling. Both Canon and Minolta implemented contact-based systems using spring-loaded gold pins on the camera side and matching contact surfaces on the lens, connected to a memory chip housed inside the lens. While Minolta employed a digital protocol, Canon relied on analog signals that modulated resistance or voltage levels for communication [6], [9], [10], [11].

Despite demands for higher data rates and storage capacity in modern digital imaging, the bayonet mount remains a robust and reliable standard, demonstrating continued relevance due to its established design and storage versatility [4].

B. Lens identification approaches for IR systems

Teledyne FLIR [12] and Telops [13] are among the most relevant providers of thermal imaging and infrared cameras. Teledyne FLIR is the market leader and offers a broad portfolio, including motorized lenses with automatic focus and lens detection via the FLIR FPO-M connector. This technology is primarily used in high-end and research systems and is based on bayonet interfaces with contact pins, similar to VIS cameras. Telops, on the other hand, serves niche markets and also uses thread and bayonet connections, but without automation. The lens data must be entered manually. Overall, automated detection systems offer decisive advantages, particularly in the high-quality IR range, with frequent lens changes and demanding applications.

Historically, companies like InfraTec, use lenses from various manufacturers utilizing the thread mount, due to compatibility benefits, with a unified set of lenses. The bayonet mount is generally not standardized since each manufacturer designs their own. This would limit companies to a specific mount manufacturer for a unified interface. Further, when using IR cameras in a static environment, the thread mount is usually sufficient. That is why thread mounts (e.g. M60 mount) are still preferred over a bayonet mount in IR context. However, thread mounted lenses are not mechanically adjustable, as they are sourced externally, but custom designs allow adjustable parameters. That is why automatic lens identification offers great potential for IR M60 interfaces.

III. Requirements for lens identification

The design and evaluation of methods for an automatic lens identification system (Section IV, V) depends on several functional requirements, which are critical for performance and integration of the system:

(1) **Precise lens detection** Due to possible manufacturing tolerances of threaded IR-lenses, lens orientation in the camera socket varies for each screwing process of the same lens. Thus, the identification system must detect lenses reliably, regardless of the rotational alignment.

(2) **High degree of lens individualization** A wide range of M60 lenses is commonly used with IR cameras, requiring accurate identification to ensure the selection of appropriate calibration data. Unrecognized lenses should be detected and measurement inaccuracies highlighted.

(3) **High durability** The system must endure up to 5,000 mechanical cycles (2,500 lens changes, assuming 5 per day over 2 years) without attrition, particularly in configurations involving electrical contacts.

(4) **Compact, hardware-efficient design** To minimize complexity, cost and time, the system should offer minimal and efficient hardware modifications or extensions, especially for module 0, supporting existing designs.

(5) **Reliable signal transmission** Robust communication between lens and camera is pivotal. This includes minimizing electromagnetic interference (EMI) and avoiding electrical shorts with the interface.

(6) **Backward compatibility** The solution must allow interfacing with previous camera-systems (i.e. module 0 connection with various lenses).

IV. Evaluation of methods for lens identification

Since the final design should not be visible or accessible from the outside, hardware should not be attached to the camera's outer surface. Further, the camera lenses cannot be mechanically adjusted, so their existing geometry must be used. Hence, the most promising implementation area is on top or inside the contact surfaces of the lens and module 0 (Fig. 1). This setup would hide the hardware internally and allow for automatic lens detection through the lens screwing process. The following selection of methods for lens identification orientates at this very interface. A distinction is drawn between contact-based and contactless realizations.

A. Contact-based lens identification method

The term contact-based method refers to mechanical elements that enable signal transfer.

The approach for a contact-based method provides for the use of a **lens-side slip ring** (Fig. 3) and spring contact tips (pogo pins) on the camera side. These spring-loaded ball-head pins enable a stable electrical connection with reduced wear on contact materials from repeated lens mounting [14]. The method integrates a slip ring and an Electrically Erasable Programmable Read-Only Memory (EEPROM) on the lens-side PCB, storing lens-specific data without needing power, enabling camera-side identification. The slip ring, in combination with spring contacts, ensures signal transmission. A one-wire protocol may be used to reduce wiring and cost, allowing power and data to share the same line, with the ground path running through the lens thread.

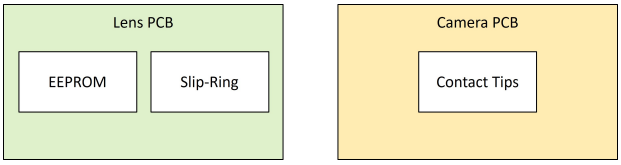

Fig. 3. Illustration of the lens-side slip ring utilization method.

B. Contactless lens identification methods

Subsequently, three distinct contactless data transfer methods, each based on a unique physical principle, are presented.

The first contactless method uses **RFID scanning** (Fig. 4) technology, replacing the previous electromechanical contacting with a radio transmission system. Two plane-parallel, circular antennas are used to enable reliable data transmission between lens and camera. A lens-side PCB includes the antenna as well as a passive, programmable RFID tag, which stores lens-specific information. The tag sources its energy from the electromagnetic field of the RFID reader in the camera and sends back the encoded data via back-scattering. The camera-side unit contains an identical antenna and an RFID reader that receives the signal, decodes it and transmits the data to a micro-controller for further processing.

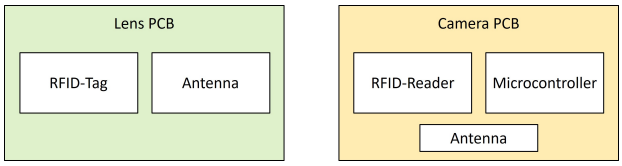

Fig. 4. Illustration of the RFID method.

Another method for contactless data transfer is the use of **magnetic encoding** (Fig. 5), where magnetic fields are detected using Hall sensors. On the lens-side PCB, magnets with patterns of different strength and orientation are used to distinguish the lenses from each other. The PCB is positioned along the lens thread. The camera side features a recessed area to house a second PCB with circularly arranged Hall sensors, placed slightly below the steel ring surface. The parallel configuration offers detection and conversion of magnetic fields into electrical signals.

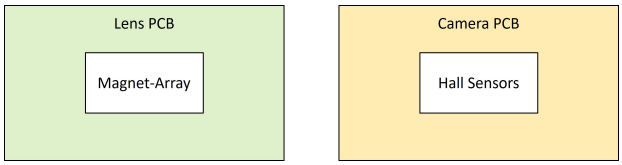

Fig. 5. Illustration of the magnetic encoding method.

The final method evaluated is **bar-code encoding** (Fig. 6), where lens data is stored in a bar-code and read by scanning. A bar-code is either affixed to or engraved into the lens in a 360° layout to ensure readability from any rotational position. This results in a slightly different geometry, using the outer body of the lens rather than the ring structure inside of the contact surface. A scanner with an integrated LED is installed in the camera's base module. Each time a lens is mounted, the bar-code is automatically scanned.

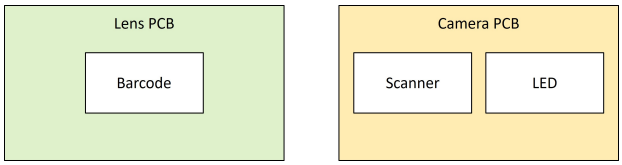

Fig. 6. Illustration of the bar-code encoding method.

For each approach, electric signals of the camera-side PCB are transferred to the existing camera-hardware via flex-cable.

V. Result comparison of evaluated methods

Using an objective comparison, based on weighted criteria, the individual methods get assessed, determining the most promising solution for the functional demonstrator.

TABLE I
EVALUATION MATRIX OF THE DIFFERENT VARIANTS FOR AUTOMATIC LENS IDENTIFICATION (ACCORDING TO VDI 2225 AND UTILITY ANALYSIS)

Evaluation criteria	**Weighting factor**		**Slip-ring**				**RFID**				**Magnetic encoding**				**Barcode**			
	VDI	***Utility***	***VDI***	***VDI w***	***Util***	***Util w***	***VDI***	***VDI w***	***Util***	***Util w***	***VDI***	***VDI w***	***Util***	***Util w***	***VDI***	***VDI w***	***Util***	***Util w***
Req. 1	0.26	0.20	3	0.78	7	1.4	4	1.04	8	1.6	3	0.78	6	1.20	3	0.78	6	1.20
Req. 2	0.20	0.22	4	0.8	9	1.98	4	0.8	9	1.98	3	0.60	6	1.32	3	0.60	6	1.32
Req. 3	0.17	0.21	2	0.34	5	1.05	4	0.68	8	1.68	3	0.51	7	1.47	3	0.51	6	1.26
Req. 4	0.06	0.06	1	0.06	3	0.18	1	0.06	3	0.18	1	0.06	3	0.18	1	0.06	3	0.18
Req. 5	0.30	0.29	3	0.90	7	2.03	4	1.2	8	2.32	3	0.90	6	1.74	3	0.90	7	2.03
Req. 6	0.01	0.02	3	0.03	6	0.12	4	0.04	9	0.16	3	0.03	6	0.12	3	0.03	7	0.14
$\sum =$	1	1	16	2.91	37	6.76	21	3.82	45	7.92	16	2.88	34	6.03	16	2.88	35	6.23
Predicate	/	/	/	Good	/	Good	/	Very good	/	Very good	/	Good	/	Good with deficits	/	Good	/	Good with deficits

For better visibility in the subsequent weighting table as well as in the utility analysis, the requirements of section III are abridged. Table II compares each of the requirements in the first row to each of the entries in the first column, respectively. The ranking ranges from 0 (less important), 1 (equally important) to 2 (more important). For the utility analysis, a target system with multiple stages (Fig. 7) is created to characterize the weighting requirements differently.

TABLE II
WEIGHTING FACTORS ACCORDING TO RANKING TABLE FOR LENS IDENTIFICATION REQUIREMENTS (ACCORDING TO VDI 2225)

	Weighting of lens identification requirements					
	Req. 1	***Req. 2***	***Req. 3***	***Req. 4***	***Req. 5***	***Req. 6***
Req. 1		0	0	0	2	0
Req. 2	2		1	0	1	0
Req. 3	2	1		0	2	0
Req. 4	2	2	2		2	0
Req. 5	0	1	0	0		0
Req. 6	2	2	2	2	2	
$\sum 30 =$	8	6	5	2	9	0
Relative %	26.7	20	16.7	6.7	30	0
Fixing	0.26	0.2	0.17	0.06	0.3	0.01

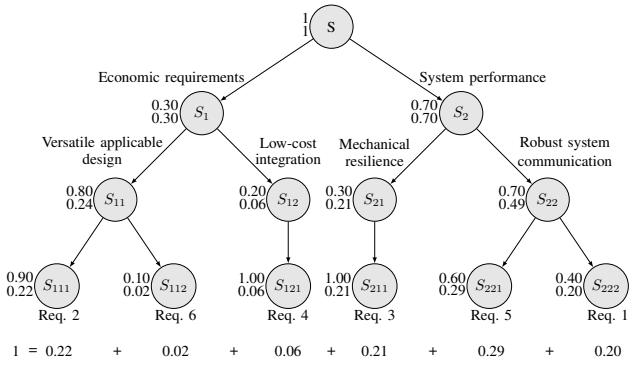

Fig. 7. Utility analysis for weighting lens identification requirements

Both comparison techniques result in weighting factors, which are multiplied by their respective value scales, ranging from 0 to 4 (as defined in VDI 2225) or from 0 to 10 (utility analysis) — with 0 representing the lowest score possible. The overall results are displayed in table I with their predicate. Every single method among the four has its own advantages and disadvantages. Method 1 (**lens-side slip ring**) shows solid results due to its use of programmable memory and mechanical reliability under rotation. Nevertheless, susceptibility to long-term wear and material sensitivity remain significant concerns. Method 2 (**RFID scanning**) shows the best results, since its not only very robust but also offers a contactless design and reliable data transmission. Albeit its hardware complexity and environmental sensitivity is relatively high. Method 3 (**magnetic encoding**) provides versatile lens-individualization and low wear rate. Yet, it is constrained by the detection range, encoding capacity and is susceptible for interference issues. Lastly, method 4 (**bar-code encoding**) offers cost-effective lens-individualization and mechanical endurance, nevertheless its performance depends on the reliable readability of the bar-code and further requires structural adjustments.

These perceptions align well with the results of the evaluation matrix. As a result, the RFID scanning method is selected for the practical implementation.

VI. REALIZATION OF THE FUNCTION DEMONSTRATOR

The design of a functional demonstrator for automatic lens identification is based on HF-RFID technology. Due to missing simulation environment, the system is validated through a physical setup using self-built components (antennas) and commercial ones (tag,reader, micro-controllers). The testing setup comprises an RFID tag attached to the lens PCB, an antenna system on both lens and camera sides, and an evaluation kit by Beta-Layout [15], featuring a HF-RFID module, transmission antenna [16] and board [17]. The ST25TA02KB-D RFID tag by ST-Electronics [18] assesses the antenna's signal transmission range as well as efficiency. The setup and results are discussed in sections VI-B and VI-C.

A. Antenna design

Given that the application demands only short-range tag detection, the operating frequency is set to $13.56\,\mathrm{MHz}$, a standard in high-frequency RFID systems. The tag and antenna system were modeled using equivalent electrical circuits that include internal resistances (R_{Chip}, R_{ant}), tuning (C_{Chip}) and stray capacitances (C_{ant}), and self-inductance (L_{ant}), arranged in parallel, leads to the resulting antenna impedance:

$$\underline{Z}_{ant}(\omega) = [\frac{1}{R_{ant}} + j \cdot \left(\omega C_{ant} - \frac{1}{\omega L_{ant}}\right)]^{-1}. \quad (1)$$

At resonance frequency ($f = f_0$), reactive components cancel out, and the impedance becomes purely resistive, which maximizes energy transfer efficiency. Since the system operates close to this resonance, the influence of the stray capacitance remains significant. Hence, an effective inductance (L_A) and an effective resistance (R_A) are defined. The resistance R_A includes both R_{ant} and minor loss contributions $R_{X,ant}$. The simplified antenna model becomes

$$\underline{Z}_{ant} = R_A + j\omega L_A, \tag{2}$$

and the equivalent circuit diagram is displayed in figure 8. The open-circuit voltage (V_{OC}) generated in the antenna

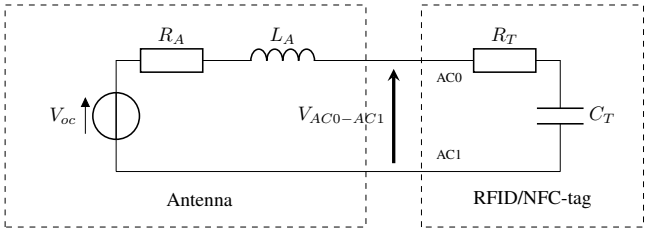

Fig. 8. Equivalent circuit diagram of RFID tag with antenna for high frequencies, according to [19]

depends on the magnetic field strength, number of coil turns, and antenna geometry. The antenna was physically constrained to a ring-shaped PCB, fitted between camera components with an approximate radial width of 7.3 mm, derived from the mechanical dimensions of the assembly (outer diameter (d_{out}): 70.3 mm, inner diameter (d_{in}): 61.6 mm).

Inductance calculations were carried out using the Saturn PCB Toolkit [20] and the modified Wheeler formula [21] [22],

$$L_{zirk} = 31.33\mu_0 n^2 \frac{a^2}{8a + 11c}, \tag{3}$$

which considers the average radius ($a = 0.25 \cdot (d_{in} + d_{out})$), number of turns ($n$), and coil width ($c = 0.5 \cdot (d_{out} + d_{in})$). Fine-tuning was achieved by adding a parallel tuning capacitor (C_{tun}) to ensure precise resonance at 13.56 MHz and thus optimal energy transfer, signal strength, and minimized reflection losses [23].

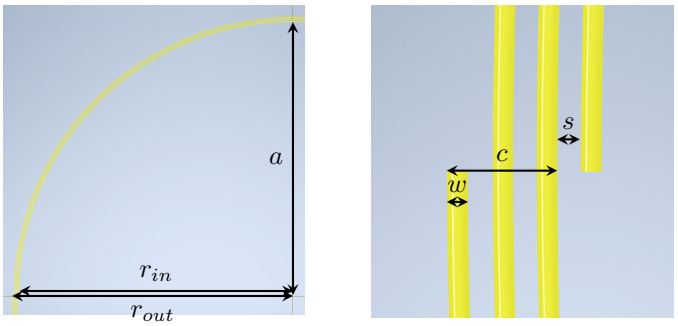

Fig. 9. Antenna dimensions

The resulting antenna layout, designed in Autodesk Inventor 360 (Fig. 9), serves as the reference for the impedance matching process and external circuit integration of the standalone antenna.

Matching Networks When designing an antenna, which is opted to interface with external hardware via a coaxial cable, the use of impedance matching is crucial to minimize signal reflections and maximize transmission efficiency. For the tests with the function demonstrator (VI-B), the antennas are evaluated in terms of transmission range (antenna with tag) and transmission performance (only antenna). In case of the transmission performance tests, the RFID-tag is omitted, thus only the antenna itself needs to be matched to to 50 Ω with the following criteria need to be fulfilled: For this application, the matching network of the measurement series needs the two criteria to be fulfilled:

- magnitude of $|Z_{ant}|$ must equal 50 Ω,
- signal transmission should be maximized at 13.56 MHz.

This is achieved by using series and parallel configurations of capacitors and inductors to tune both the resistance and reactance. The antenna's equivalent impedance is given by

$$\underline{Z}_{ant} = R_A + j\omega L_A \approx (R_{ant} + R_{rad}) + j\omega L_A. \tag{4}$$

The radiation resistance (R_{rad}) is negligible and the antenna resistance (R_{ant}) is calculated as

$$R_{ant} = \rho \cdot \frac{l_{ges}}{A_{conductor}}, \tag{5}$$

with $\rho = 1.78 \times 10^{-8}\,\Omega\,\mathrm{m}$, the conductor length $l_{ges} \approx 629.7\,\mathrm{mm}$, and the squared cross-sectional area $A_{conductor} = w \cdot D_{Cu} = 4.375 \times 10^{-9}\,\mathrm{m}^2$. This ultimately results in $R_{ant} \approx 2.56\,\Omega$ and an inductive reactance at 13.56 MHz with $X_L = \omega L_A \approx 141.39\,\Omega$.

For the determination of the matching network a normalized Smith Chart [24], [25] ($\underline{Z}_{norm}$) is used with a 50 Ω reference:

$$\underline{Z}_{norm} = R_A + j\omega L_A \approx 0.05 + j \cdot 2.83. \tag{6}$$

A series capacitor is used to cancel the reactive component $j \cdot 2.83$, bringing the impedance to the real axis with $C_{tun} \approx \omega X_C \approx 83.01\,\mathrm{pF}$. From this point, a series resistor brings the impedance to the center of the Smith Chart with $R_{tun} = 0.95 \cdot 50 \approx 47.45\,\Omega$.

While resistors generally introduce power loss, their use here ensures robustness against component tolerances, which can be significantly higher for capacitors and inductors. The

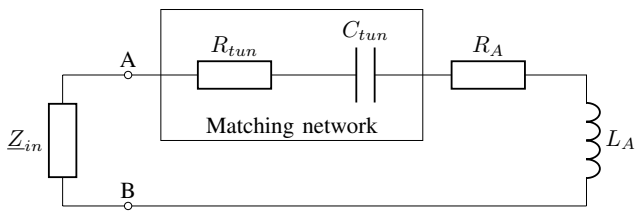

Fig. 10. Equivalent circuit for antenna and corresponding matching network.

resulting equivalent circuit (Fig. 10) is implemented on a PCB designed in Altium (Fig. 11), including also the drawing

exchange format (DXF) file of the spiral antenna layout. The modular designed board includes SMA connectors, component footprints for tuning, test points, and an RFID tag interface, offering performance validation and future optimization.

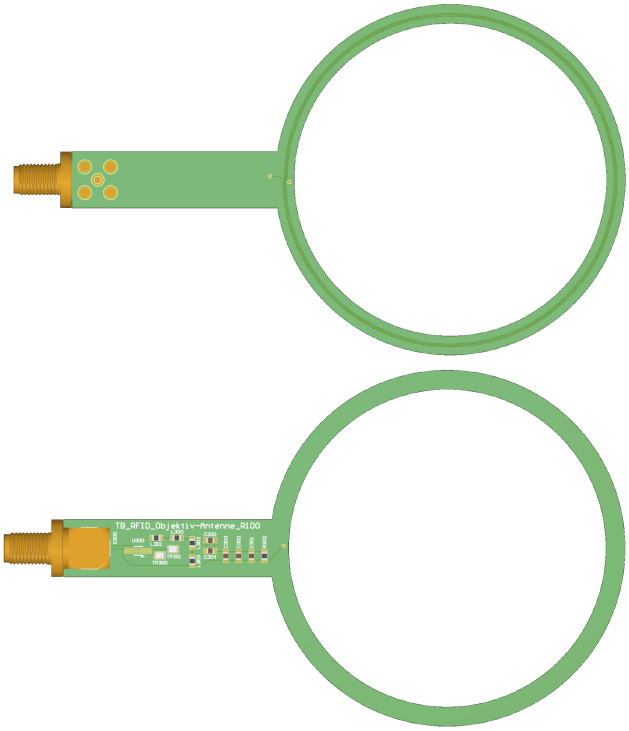

Fig. 11. PCB design of high frequency (HF) RFID antenna

B. Antenna transmission range and efficiency measurements

To validate the demonstrator's functionality, transmission measurements are conducted using a Rigol DSA875 spectrum analyzer [26], isolating antenna performance by excluding RFID tags and readers. The setup employs $50\,\Omega$ matching networks and consists of two PCB antennas connected via coaxial cables -one fixed, one movable- mounted on a micrometer-guided table with a 3D-printed adapter. The analyzer's tracking generator enables frequency-dependent loss measurements.

Prior to the series of measurements, calibration checks, using a loop-back configuration and an RF demo kit with known reference filters, confirmed accurate instrument operation. The measurement parameters included a power level of $-3\,\mathrm{dBm}$, a frequency span of $100\,\mathrm{kHz}$ to $85\,\mathrm{MHz}$, a resolution bandwidth of $120\,\mathrm{kHz}$, and a sweep time of $11.55\,\mathrm{ms}$.

Various material combinations (e.g. steel-steel, aluminum-steel, etc.) are tested due to the camera's mixed component-part environment (Fig. 12). The air–air configuration shows the best transmission at a $2.0\,\mathrm{mm}$ antenna spacing (Fig. 13).

Additionally, RFID transmission range is evaluated using a standalone antenna with a tag-specific matching circuit. The receiving setup includes transmission antenna, RFID module (coaxially connected) and evaluation kit. A maximum air-transmission range of approximately $7\,\mathrm{cm}$ is achieved.

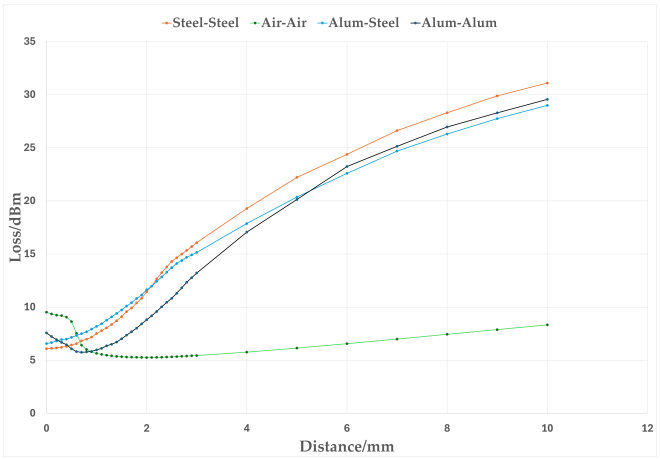

Fig. 12. Attenuation characteristics of the various materials.

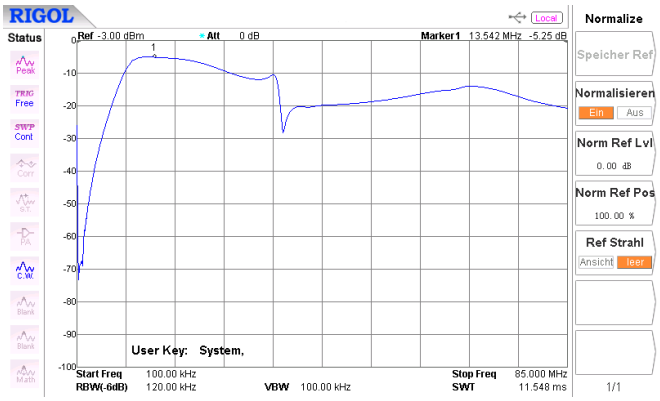

Fig. 13. Optimal transmission power loss curve.

C. Evaluation of the measurement results

The RFID HF PCB antenna's transmission performance was evaluated based on measured data (Fig. 13). Maximum signal transmission occurred near $13.54\,\mathrm{MHz}$. Despite the bandwidth is rather big and hence disadvantageous from a theoretical perspective, the result is practically not avoidable and even expected when considering the formula for the quality factor of the series-resonant circuit (Fig. 10):

$$Q = \frac{1}{R}\sqrt{\frac{L}{C}} = \frac{1}{R_{tun} + R_A}\sqrt{\frac{L_A}{C_{tun}}} \approx 2,825. \qquad (7)$$

The value lies within the expected range for broadband systems ($1 \leq Q \leq 10$), indicating robust and stable transmission. An anti-resonance effect is observable around $34\,\mathrm{MHz}$, likely due to parasitic interactions between antenna and PCB layers. Since it is well outside the operational frequency, its effect is negligible. Figure 12 compares material pairings, showing best performance in the air–air configuration, particularly within $1.5\,\mathrm{mm}$ and $3.5\,\mathrm{mm}$ spacing, indicating efficient impedance matching. The aluminum combination shows a distinct minimum in losses (optimal spacing) due to optimal coupling at around $1\,\mathrm{mm}$, before the increase of losses rises gradually.

The steel configurations exhibited steadily increasing losses, likely due to a more stable magnetic field coupling.

Assuming a $20\,\mathrm{dBm}$ generator output and negligible cable losses, the antenna's minimum power loss at $13.54\,\mathrm{MHz}$ results in $P_{\mathrm{ant}} \approx 3.35\,\mathrm{mW}$. With the supplied power of the tracking generator ($P_{\mathrm{app}} = 100\,\mathrm{mW}$), the antenna's efficiency calculates as 96.65%. This corresponds to a very good efficiency for the optimal transmission frequency.

Reliable RFID communication is detectable up to $7\,\mathrm{cm}$, with losses of roughly $35\,\mathrm{dB}$. For steel–steel configuration at $1\,\mathrm{cm}$ the maximum attenuation of $31.10\,\mathrm{dB}$ is still under the threshold of the maximum RFID range. The maximal available space inside the camera amounts to $5\,\mathrm{mm}$, which is far less compared to the $1\,\mathrm{cm}$, being evaluated. Thus, the results confirm that the antenna meets the spatial and performance requirements of the application.

Potential improvements include replacing resistors with other passive components, optimizing PCB layout for slightly narrower bandwidth, adding ground planes for better current return paths, and ensuring symmetrical design to minimize reflective losses and improve parallel alignment of antennas during testing to reduce calibration errors.

VII. Summary and Outlook

This study presents several methods for enabling automatic lens identification for IR cameras with a M60 thread mount interface. Hereby, a lens extension is required to reduce calibration errors and improve the system's user-friendliness for the costumer. Of all the solutions evaluated, the contactless RFID-based approach was identified as the most promising, verified by the functional demonstrator.

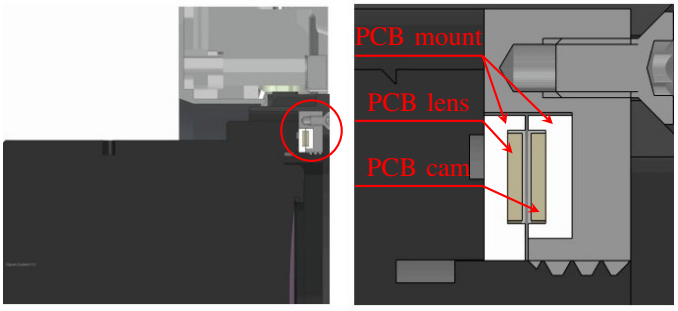

Fig. 14. Vertical sectional view of module 0 for implementing the RFID solution in existing camera architecture.

The completed study provides a foundation for future implementations in prototype development for thermographic cameras. Carrying out mechanical modifications to both the camera housing and the lens mount in order to integrate the two PCB rings is proposed. Special attention is given to maintaining precise alignment, even in the presence of manufacturing tolerances (Fig 14). Further, the RFID tag can be embedded into the PCB to minimize the risk of damage and save space. Finally, an additional PCB with integrated RFID reader and micro-controller should be developed for reliable data transfer with the camera-side antenna. Altogether, future integration of the prototype into the camera system could significantly streamline radiometric calibration by offering automatic detection of lens parameters.

Acknowledgment

The author would like to thank Fabian Göttfert and the mechanical department of the company InfraTec GmbH for the technical support as well as for providing the environment and the current camera model to make this work possible.

References

[1] "InfraTec GmbH website," https://www.infratec.eu/thermography/ (accessed 04/06/2025).
[2] H. Budzier and G. Gerlach, "Thermische Infrarotsensoren Grundlagen für Anwender," 1st ed. Berlin: *Wiley-VCH*, 2010, ISBN 3-527-40960-2.
[3] D. Walther, "Lens mounts in comparison - bayonet, thread, clamping ring," https://fotowalther.de/objektivanschluesse-bajonett-mount-klemmring-breech-lock-gewinde-screw-thread/ (accessed 04/06/2025).
[4] M. Pritchard, "A history of photography in 50 cameras," 1st ed. London: *Bloomsbury*, 2014, ISBN 9781472575388.
[5] M. Gradias, "Nikon Fotografie," 1st ed. Munich: *Markt & Technik*, 2010, ISBN 978-3-8272-4653-0.
[6] B. Shell; G. Richter, "Canon-Handbuch: Das komplette Canon System von Gestern bis Heute," 1st ed. Munich: *Laterna Magica*, 1994, ISBN 3874675432.
[7] N. Stephan, "The M42 Mount - History, Cameras, and Adapting the Lens Mount," https://www.outsidetheshot.com/m42-mount/ (accessed 04/06/2025).
[8] T. Thomas, "Special feature of M42 lenses: open aperture metering & working aperture metering," https://analoge-fotografie.net/blog/m42-objektive-offenblendmessung (accessed 04/06/2025).
[9] G. Lepp; J. Dickerson, "Canon-Objektive," 1st ed. Munich: *Markt & Technik*, 1996, ISBN 3874676773.
[10] A. Decker, "Minoltas Triumph - die 7000 AF : Viele experimentierten - einer schafft es," *Photo deal*, 2005, 3 pp. 56-59.
[11] "Minolta 7000 Service Manual," https://www.manualslib.com/download/3478893/Minolta-7000.html (accessed 04/06/2025).
[12] "Teledyne FLIR website," https://www.flir.de/ (accessed 04/06/2025).
[13] "Telops website," https://www.telops.com/ (accessed 04/06/2025).
[14] C.C.P. Contact Probes Co., LTD. "Pogo Pin Connectors," https://www.ccpcontactprobes.com/pogo-pin-connectors(accessed 11/06/2025).
[15] KTS GmbH, "Data sheet Evaluation Board for RFID Module," *Rev: 20150724*, Jul. 2015. (accessed 20/06/2025).
[16] KTS GmbH, "Data sheet RFID HF PCB Antenna," *Rev: 20130903*, Sep. 2013. (accessed 20/06/2025).
[17] KTS GmbH, "Data sheet RFID HF Module," *Rev: 20130913*, Sep. 2013. (accessed 20/06/2025).
[18] STMicroelectronics, "NFC Forum Type 4 Tag IC with up to 2-Kbit EEPROM," *DS12365 - Rev 2*, Sep. 2018. (accessed 03/06/2025).
[19] STMicroelectronics, "Application note: How to design a 13.56 MHz customized antenna for ST25 NFC / RFID Tags," (accessed 19/06/2025).
[20] Saturn PCB Design, Inc., "Saturn PCB Design Toolkit Version 8.41," https://saturnpcb.com/saturn-pcb-toolkit/ (accessed 04/06/2025).
[21] H. A. Wheeler, "Simple Inductance Formulas for Radio Coils," *Proceedings of the I.R.E.*, Oct. 1928.
[22] M. T. Thompson "Inductance Calculation Techniques," *Power Control and Intelligent Motion*, Dec. 1999.
[23] A. Petrariu; V. Popa, "The Role of Impedance Matching for Power Transfer Efficiency in HF RFID Systems," *9th International Symposium on Advanced Topics in Electrical Engineering (ATEE)*, May. 2015.
[24] M. Rotaru; G. Rezmeriță; I. Mihăilă; M. Popescu; M. Iordache, "Presentation of the Smith Chart and Applications to Analog Circuit Analysis," *The 13th International Symposium on Advanced Topics in Electrical Engineering*, Mar. 2023.
[25] U. Siart, "Quick guide to the Smith chart," http://www.siart.de/lehre/smishort.pdf (accessed 03/06/2025).
[26] Rigol Technologies, Inc., "Data sheet DSA875 Series 7.5 GHz Spectrum Analyzer," Jul. 2017. (accessed 20/06/2025).